Supplemental Information

Dynein-Mediated Regional Cell Division

Reorientation Shapes a Tailbud Embryo

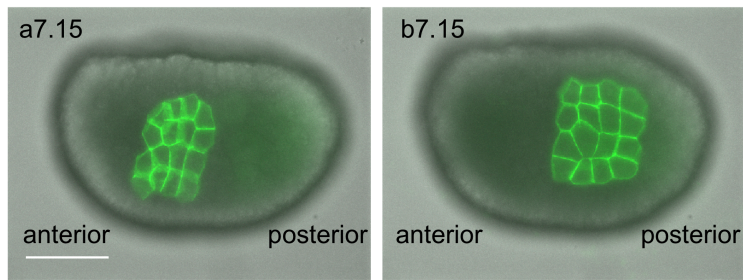Ayaki Nakamoto and Gaku Kumano

Figure S1 (related to Figure 1)
The 11th epidermal cell division. Lateral side view, with anterior to the left. Scale bar, 100 μm. Either trunk epidermal precursor cell (a7.15) or tail epidermal precursor cell (b7.15) was injected with PH-YFP mRNA at the 64-cell stage (i.e., after the 6th division stage), and the number of descendants before the formation of epithelial bending was calculated. Both labeled cells divided to produce 16 cells (i.e. four times), indicating that the 10th division had been completed. Thus, the division during the formation of epithelial bending is the 11th. Also, the resulting squares of 4 × 4 cells may suggest that a7.15 and b7.15 underwent 4 rounds of alternate cell divisions at right angles to each other, highlighting a specific cell cycle undergoing division reorientation at the 11th division.
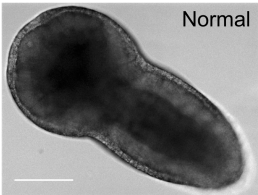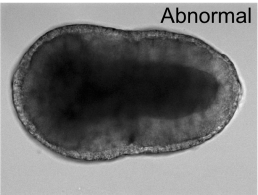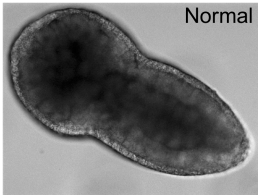
	Control 0.4% DMSO for 1 h (n=12)	30 μM Ciliobrevin D for 1 h (n=15)	10 μM Ciliobrevin D for 2 h (n=19)
Start of division (average ± s.d.)	NR+1 h 27 min ± 8 min	NR+2 h 57 min ± 4 min	NR+3 h 24 min ± 12 min
End of division (average ± s.d.)	NR+3 h 6 min ± 15 min	NR+5 h 3 min ± 7 min	NR+5 h 25 min ± 7 min
Period of the division	1 h 39 min	2 h 06 min	2 h 1 min
Epithelial bending			

Figure S2 (related to Figure 1)
Effect of dynein inhibitor on cell division timing. Table showing the start of the cell division (top), the end of the cell division (middle), and the period of the cell division (bottom). The period of the division was calculated by subtracting the average of the start of division from the average of the end of the division. Scale bar, 100 μm. The definition of the start and the end of cell division is described in the methods section. Resultant tailbud embryos are shown under the table.
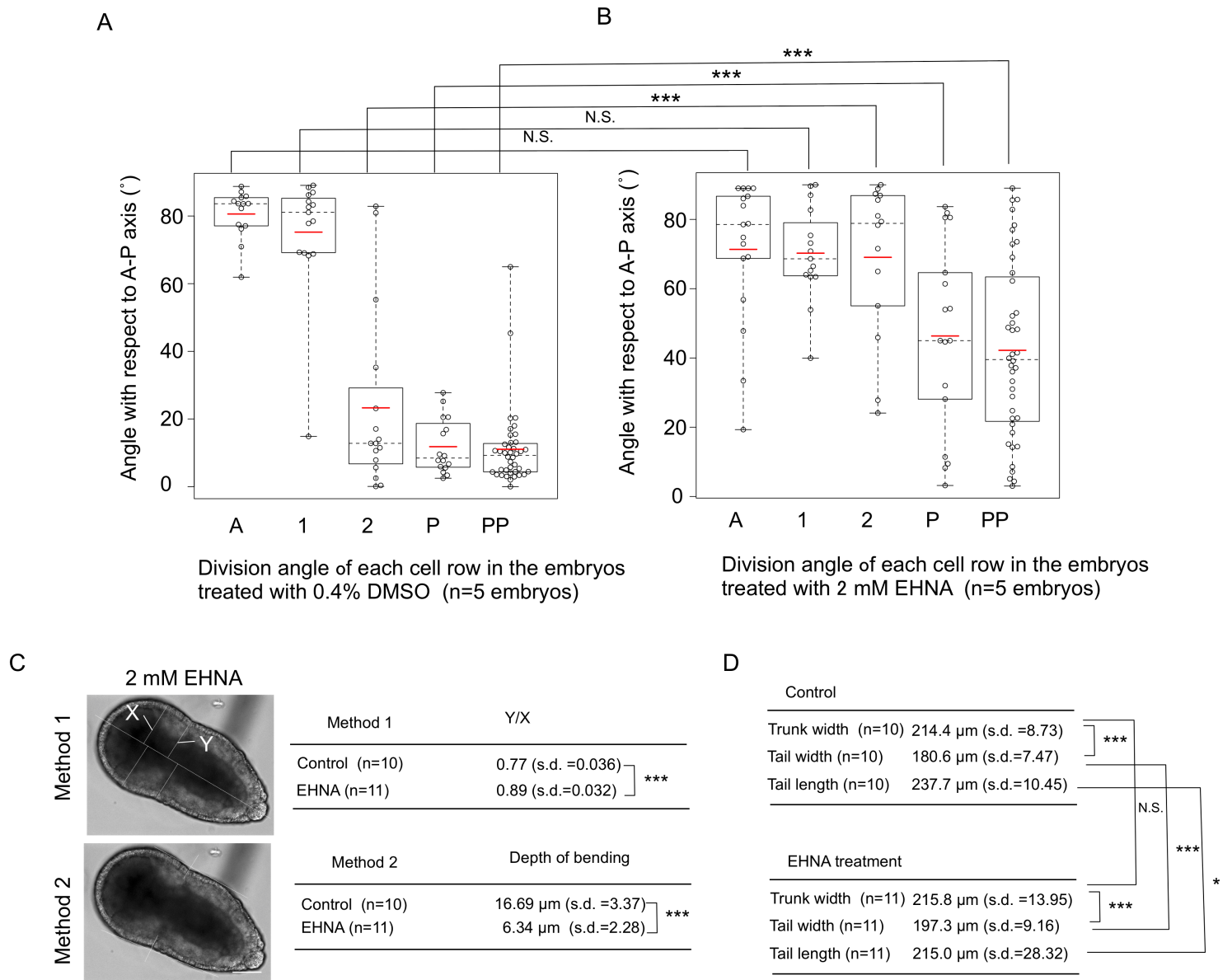
Figure S3 (related to Figure 4)
Effect of dynein inhibitor EHNA on pattern of epidermal cell division and formation of epithelial bending. (A, B) Angle of division orientation with respect to the A–P axis in the DMSO-treated control (A) and EHNA-treated embryos (B). The DMSO-treated embryos (n=5, Fig. 4B) were used as the control. In the EHNA-treated embryos (n=5 embryos), the values were extracted from 17 cells for row A, 15 cells for row 1, 14 cells for row 2, 17 cells for row P and 40 cells for row PP. Data are represented as individual values and boxplots. Means are indicated as red horizontal bars. Medians are indicated with dashed lines. Boxes indicate second and third quartiles, and whiskers indicate the maximum and minimum values. There was no statistically significant difference in the cell rows A and 1 between the DMSO-treated control and EHNA-treated embryos; however, the angles of the cell rows 2, P and PP of the EHNA-treated embryos were significantly higher than those of the control embryos. N.S. and *** indicate p>0.05 and p<0.001, respectively (T-test). (C) Phenotype of EHNA-treated embryo and quantitative evaluation of the epithelial bending. See experimental procedure for the calculation methods. Table shows the results of calculations. *** indicates p<0.001 (T-test). Scale bars, 100 μm. (D) The width of the trunk and tail regions and the tail length in the DMSO-treated control and EHNA-treated embryos. See experimental procedure for the calculation methods. N.S., * and *** indicate p>0.05, p<0.05 and p<0.001, respectively (T-test).
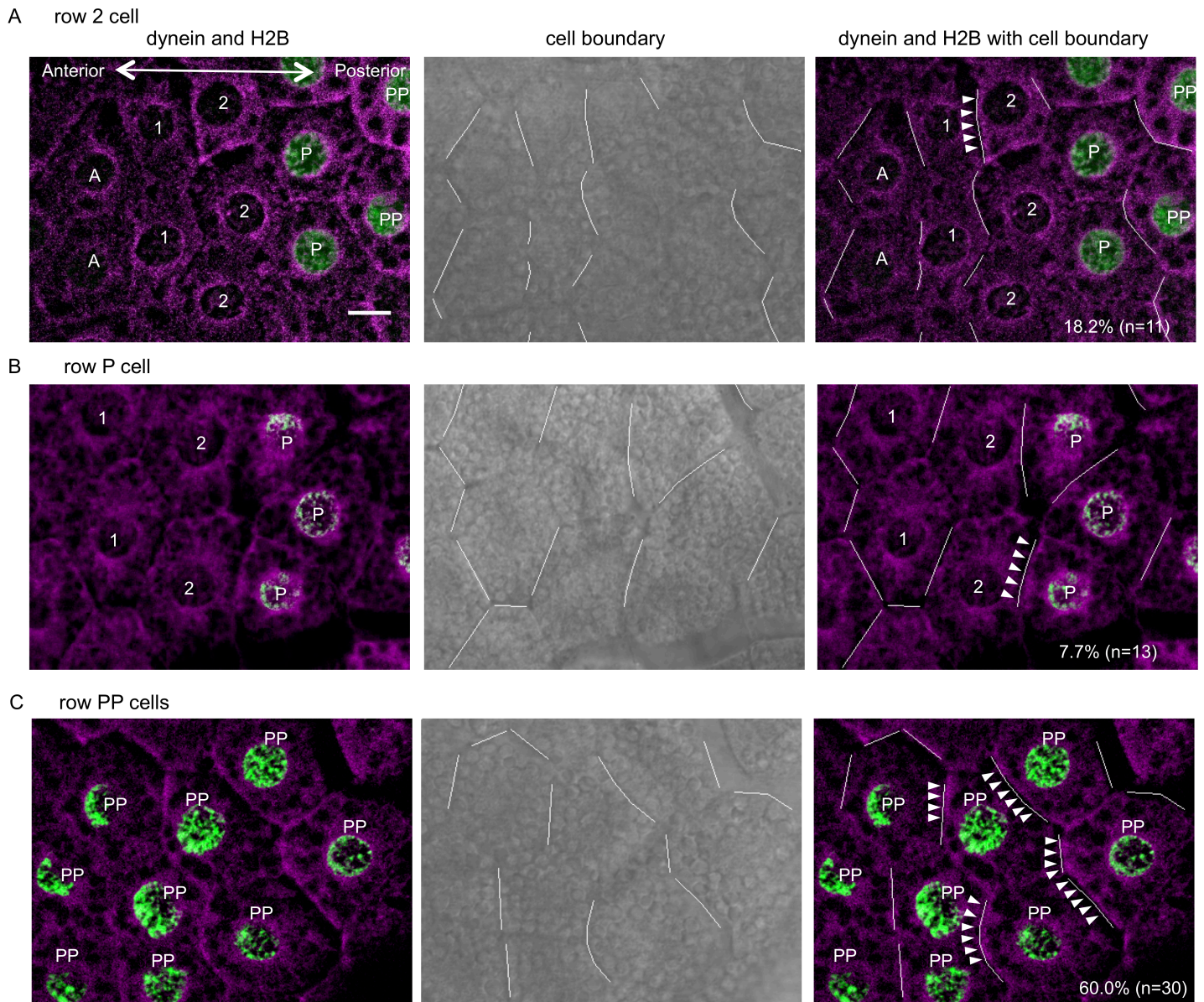
A row 2 cell

dynein and H2B — cell boundary — dynein and H2B with cell boundary

18.2% (n=11)

B row P cell

7.7% (n=13)

C row PP cells

60.0% (n=30)

Figure S4 (related to Figure 5)
Dynein protein in localization in each cell row. Image of double staining for anti-dynein and anti-GFP antibody staining (A–C). Anti-GFP antibody recognizes the nuclei of the posterior epidermal cells, which are marked by H2B-GFP. H2B-GFP mRNA has been injected into a progenitor cell of the posterior epidermal cells at the 8-cell stage embryo (b4.2). Stained embryos were squished gently to separate cell–cell contact and to identify the cell boundary (middle), which is shown by a white line. The dynein signal was indicated by arrowheads when detected in the anterior side of the cells. A, 1, 2, P and PP represent cells in row A, 1, 2, P and PP, respectively, according to the GFP expression. The digits in the bottom right in the right-hand images show the proportion of the cells in which anterior localization was observed out of the cells whose cell boundaries were identified. Scale bar, 10 μm.
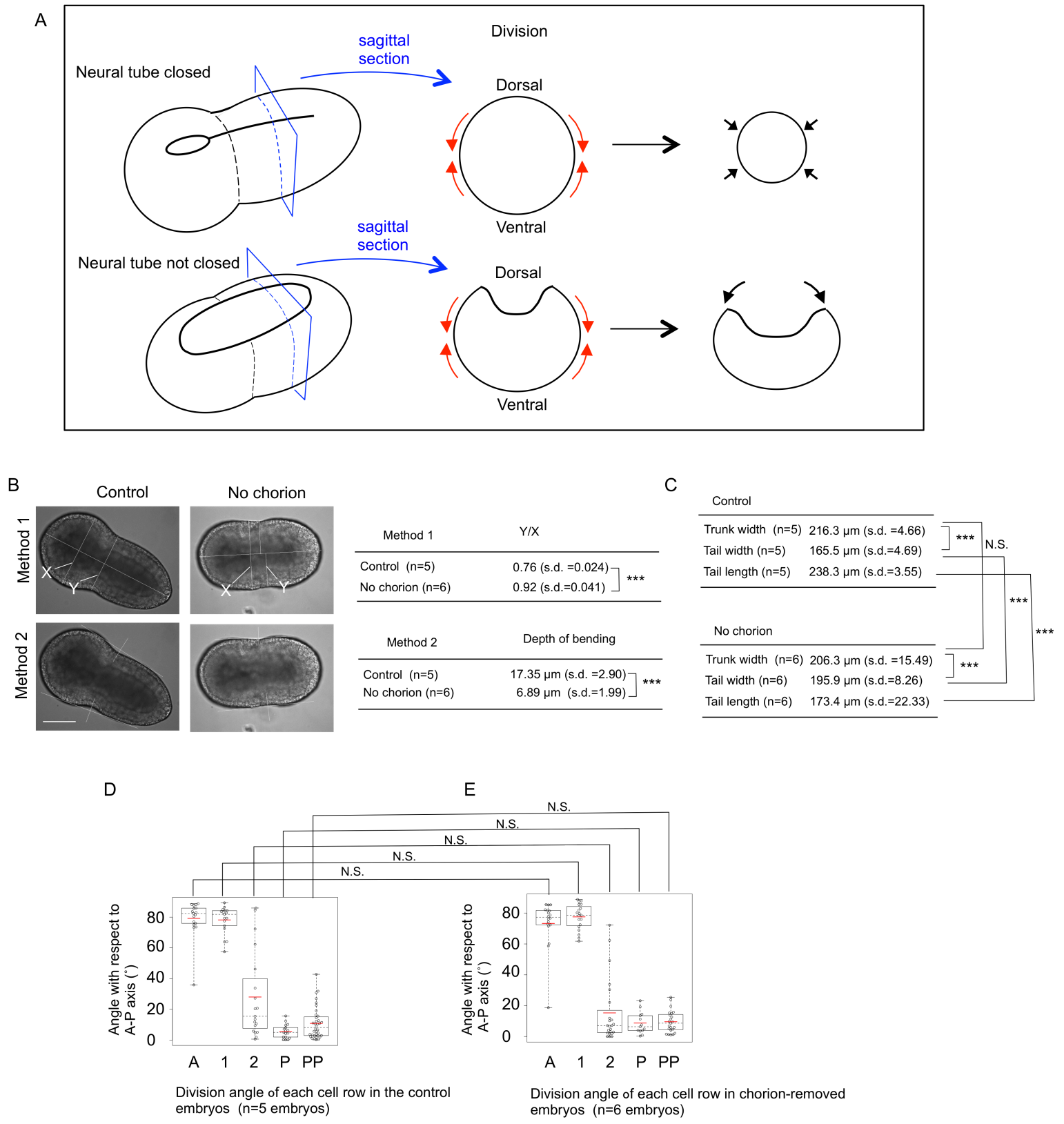
A — Neural tube closed / sagittal section / Division / Dorsal / Ventral

Neural tube not closed / sagittal section / Dorsal / Ventral

B

Method 1 — Control / No chorion

Method 2 — Control / No chorion

Method 1	Y/X
Control (n=5)	0.76 (s.d. =0.024)
No chorion (n=6)	0.92 (s.d.=0.041)

***

Method 2	Depth of bending
Control (n=5)	17.35 μm (s.d. =2.90)
No chorion (n=6)	6.89 μm (s.d.=1.99)

***

C

Control	
Trunk width (n=5)	216.3 μm (s.d. =4.66)
Tail width (n=5)	165.5 μm (s.d.=4.69)
Tail length (n=5)	238.3 μm (s.d.=3.55)

No chorion	
Trunk width (n=6)	206.3 μm (s.d. =15.49)
Tail width (n=6)	195.9 μm (s.d.=8.26)
Tail length (n=6)	173.4 μm (s.d.=22.33)

*** N.S. *** *** ***

D

N.S. / N.S. / N.S. / N.S. / N.S.

Angle with respect to A-P axis (°)

A   1   2   P   PP

Division angle of each cell row in the control embryos (n=5 embryos)

E

Angle with respect to A-P axis (°)

A   1   2   P   PP

Division angle of each cell row in chorion-removed embryos (n=6 embryos)

Figure S5 (related to Figure 6)
Effects of the chorion removal on the pattern of epidermal cell division and the formation of epithelial bending. (A) Schematic diagrams of predicted outcomes of epithelial cell divisions along the A–P axis on the thickness of the future tail region and thus the epithelial bending formation in embryos with (top) or without (bottom) the neural tube closure. Overall embryos are shown on the left with positions of sagittal sections shown on the right. Shown on the right are representatives of what might happen in the future tail region along the entire length of the region where epithelial cells divide along the A–P axis. Red arrows indicate predicted constricting forces generated around the

circumference of the embryos by the A–P oriented cell divisions. The force would not be propagated enough to constrict the circumference if it is not tied together throughout by the failure of the neural tube closure (black arrows, bottom-right). (B) Phenotype of chorion-removed embryo and quantitative evaluation of the epithelial bending. See experimental procedure for the calculation methods. Table shows the results of calculations. *** indicates $p<0.001$ (T-test). Scale bars, 100 μm. (C) The width of the trunk and tail regions and the tail length in the control and chorion-removed embryos. See experimental procedure for the calculation methods. N.S. and *** indicate $p>0.05$ and $p<0.001$, respectively (T-test). (D, E) Angle of division orientation with respect to the A–P axis in the intact control (D) and chorion-removed embryos (E). In the intact control (n=5 embryos), the values were extracted from 17 cells for row A, 17 cells for row 1, 19 cells for row 2, 17 cells for row P and 36 cells for row PP. In the chorion-removed embryos (n=6 embryos), the values were extracted from 18 cells for row A, 19 cells for row 1, 23 cells for row 2, 13 cells for row P and 23 cells for row PP. Data are represented as individual values and boxplots. Means are indicated as red horizontal bars. Medians are indicated with dashed lines. Boxes indicate second and third quartiles, and whiskers indicate the maximum and minimum values. There is no statistically significant difference between the intact control and chorion-removed embryos. N.S. indicates $p>0.05$ (T-test).
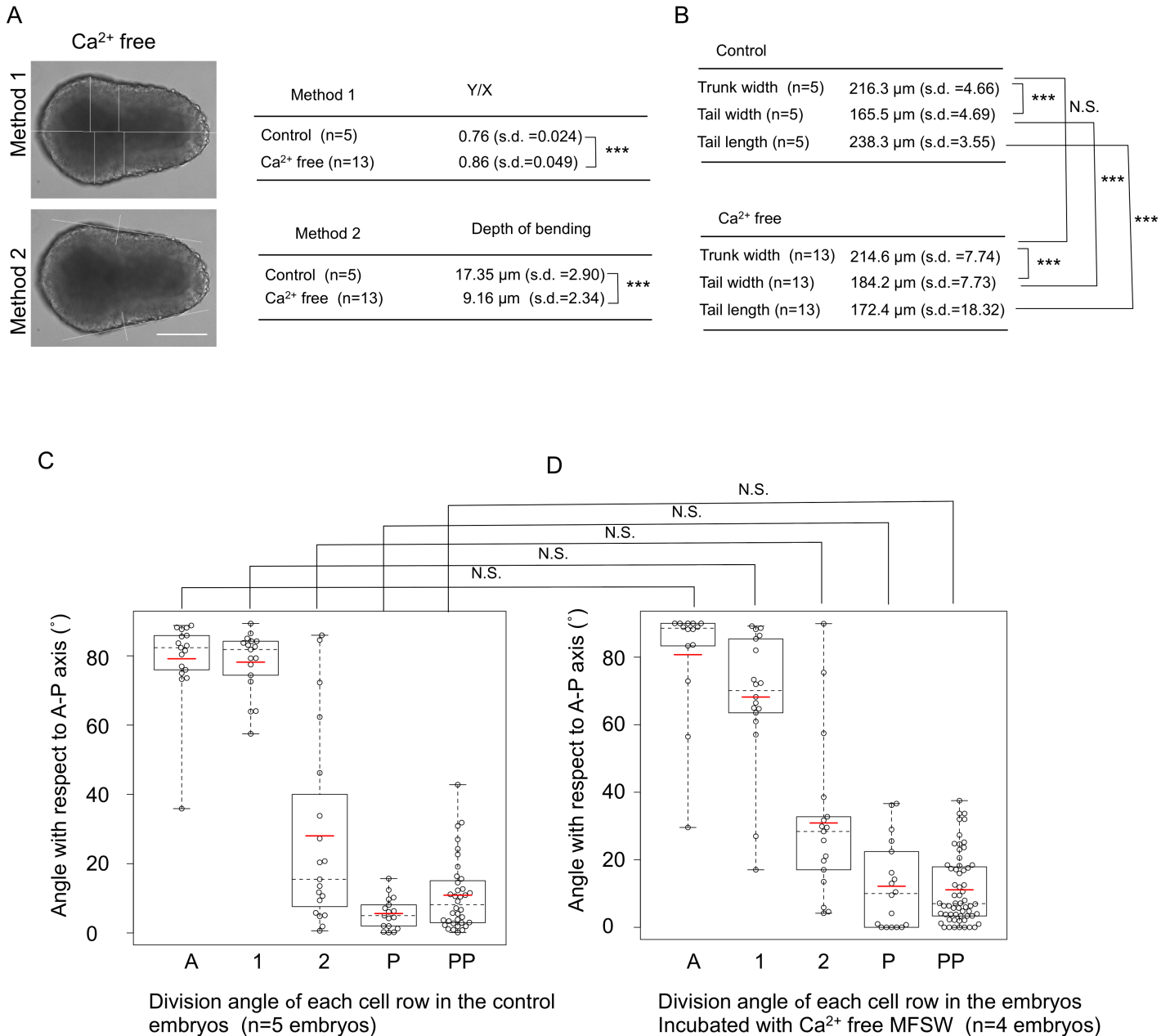
A

Ca²⁺ free

Method 1

Method 1	Y/X
Control (n=5)	0.76 (s.d. =0.024)
Ca²⁺ free (n=13)	0.86 (s.d.=0.049)

***

Method 2	Depth of bending
Control (n=5)	17.35 μm (s.d. =2.90)
Ca²⁺ free (n=13)	9.16 μm (s.d.=2.34)

***

B

Control

Trunk width (n=5)	216.3 μm (s.d. =4.66)
Tail width (n=5)	165.5 μm (s.d.=4.69)
Tail length (n=5)	238.3 μm (s.d.=3.55)

*** N.S.

Ca²⁺ free

Trunk width (n=13)	214.6 μm (s.d. =7.74)
Tail width (n=13)	184.2 μm (s.d.=7.73)
Tail length (n=13)	172.4 μm (s.d.=18.32)

*** *** ***

C

Division angle of each cell row in the control embryos (n=5 embryos)

D

Division angle of each cell row in the embryos Incubated with Ca²⁺ free MFSW (n=4 embryos)

Figure S6 (related to Figure 6)
Effect of Ca2+ free sea water on the pattern of epidermal cell division and the formation of epithelial bending. (A) Phenotype of the embryo incubated in Ca2+ free sea water and quantitative evaluation of the epithelial bending. See experimental procedure for the calculation methods. Table shows the results of calculations. *** indicates p<0.001 (T-test). Scale bars, 100 μm. (B) The width of the trunk and tail regions and the tail length in the control embryos and the embryos incubated in Ca2+ free sea water. See experimental procedure for the calculation methods. N.S. and *** indicate p>0.05 and p<0.001, respectively (T-test). (C, D) Angle of division orientation with respect to the A–P axis in the control (C) and the embryos incubated in Ca2+ free sea water (D). The intact embryos (Fig. S5D) were used as the control. In the embryos incubated with Ca2+ free sea water (n=4 embryos), the values were extracted from 14 cells for row A, 18 cells for row 1, 17 cells for row 2, 18 cells for row P and 60 cells for row PP. Data are represented as individual values and boxplots. Means are indicated as red horizontal bars. Medians are indicated with dashed lines. Boxes indicate second and third quartiles, and whiskers indicate the maximum and minimum values. There is no statistically significant difference for each cell row between the intact control and the embryos incubated in Ca2+ free sea water. N.S. indicates p>0.05 (T-test).

TRANSPALENT METHODS

Animals and embryos
We obtained adults of *Halocynthia roretzi* from local fishermen near the Asamushi Research Center for Marine Biology (Aomori, Japan). Naturally-spawned eggs were fertilized using a suspension of nonself sperm. Embryos were cultured in Millipore-filtered seawater (MFSW) containing 50 μg/ml streptomycin and 50 μg/ml kanamycin at 9–13°C.

Constructs
This study used the following constructs: DCIC-EGFP: *Halocynthia roretzi* dynein cytoplasmic intermediate chain (DCIC) was identified in the MAGEST (EST database of eggs and embryos; http://magest.hgc.jp/) and Aniseed database (Harore.CG.MTP2014.S40.g04074, https://www.aniseed.cnrs.fr/). Based on the sequences of MAGEST contig 5549, which includes the 5'UTR, and the MAGEST contig 8626, which includes the 3'UTR, the entire ORF was cloned by RT-PCR using the forward primer (5'-GAAGGATCCACCATGTCAGAAAAATCTGATCGGAAAGCT-3') and reverse primer (5'-GAACCATGGTTAATTGTCTGGCTATCAATGCCTCTTCT-3'). Template cDNA was generated from the neurula stage mRNA. The fragments of DCIC and EGFP were inserted into pBSHTB(N). MAP7-GFP: MAP7-GFP in pSPE3 was a gift from Dr. Alex McDougall. The N-terminal fragment of mouse MAP7 was used (Prodon et al., 2010). H2B-GFP: H2B-GFP in pBSHTB(N) was a gift from Dr. Takehumi Negishi. MAP7-mCherry: N-terminal fragment of MAP7 from the MAP7-GFP in pSPE3 was inserted into the EAAARx3-mCherry in pBSHTB(N) (Takatori et al., 2010). PH-YFP: A PCR fragment containing PH-YFP from Tbx6b>PH-YFP (a gift from Dr. Anna DiGregorio) was inserted into the pBSHTB(N). PH-dTomato: PH-dTomato in pBSRN3 was a gift from Dr. Alex McDougall.

mRNA synthesis and microinjection
mRNAs encoding the fusion proteins (DCIC-EGFP, MAP7-GFP, MAP7-mCherry, H2B-GFP, PH-YFP, PH-dTomato) were synthesized *in vitro* using the mMessage mMachine kit (Ambion), and poly(A) was added to the 3' ends of the synthesized mRNAs using the Poly(A) Tailing kit (Ambion) according to the manufacturer's instructions. We used the following restriction enzymes and RNA polymerases: T3 and NotI for DCIC-EGFP; T3 and SfiI for MAP7-GFP; T3 and NotI for MAP7-mCherry; T3 and PstI for H2B-GFP; T3 and NotI for PH-YFP; and T3 and SfiI for PH-dTomato. The synthesized mRNA was microinjected into fertilized eggs, a4.2, b4.2, a7.15, or b7.15 cells according to Miya et al. (1997) and Niwano et al. (2009) as described in the following. Fertilized eggs were treated with 0.05% actinase E (Kaken Pharmaceutical, Japan) in MFSW for 10 min to remove the follicle cells on the chorion. The treated eggs were washed with MFSW and transferred on the cover glass in plastic petri dish filled with MFSW. The eggs with chorion but without follicle cells were stuck on the cover glass. The solution to be microinjected was loaded in glass needles for microinjection which were made by pulling glass capillaries (GDC-1, Narishige) with a horizontal puller (PN-3, Narishige). Microinjection was carried out with a micromanipulator (MN-151, Narishige) under the dissection microscope (OLYMPUS SZX16).

Live imaging
Time lapse observation was performed using either a LSM710 Zen zeiss confocal microscope (Fig. 1C, 3A, 3B, Supplemental Movies 2 and 3) or a Nikon eclipse T*i* (Fig. 2A, 4A, 5D, 6A, Supplemental Movies 1, 4–9). For observation with the LSM710 Zen zeiss confocal microscope, embryos with vitelline membrane were mounted on the slide glass in random orientations, and well-oriented embryos were selected for observation of their lateral sides. Images were obtained every 2 min at 1.0–2.5 μm intervals. For observation with the Nikon eclipse T*i*, the vitelline membranes were removed with forceps in a plastic dish coated with 1% agarose in MFSW. The embryos were transferred to a glass-bottomed dish (Matsunami) filled with 2% methylcellulose in MFSW and carefully oriented using tungsten needles so that the lateral side could be observed. Images were obtained every 2–4 min at 4.0 μm intervals and were then subjected to deconvolution with the Nikon NIS-Elements software to reduce blurriness. The two different methods revealed the same pattern of epidermal cell divisions.

Drug treatment
Dynein inhibitor Ciliobrevin D (Calbiochem) was dissolved in DMSO at 50 mM and stored at −20°C

as a stock solution. Before use, the stock solution was diluted to 30 μM in MFSW. The embryos were treated with 30 μM Ciliobrevin D for 1 h, beginning 1 h after neurula rotation (NR) (approximately 30 min before the 11th epidermal cell divisions). In another experiment, embryos were treated with 10 μM Ciliobrevin D for 2 h, beginning 1 h after NR. Following the treatment, embryos were washed with MFSW and then either used for live-imaging, as described above, or placed under the dissection microscope (OLYMPUS SZX16) to observe the epithelial bending. The 11th cell divisions had not begun at the time of washing with MFSW. The control embryos were treated with 0.4% DMSO for 1h from the NR+1 h stage. Another dynein inhibitor, EHNA (Santa Cruz Biotechnology), was dissolved in sterilized water at 50 mM and stored at 4°C as a stock solution. Before use, the stock solution was diluted in MFSW to either 1 mM or 2 mM. At 1 h after NR, the embryos were treated with 2 mM EHNA for 1 h and then treated with 1 mM EHNA for another 30 min. The treated embryos were washed with MFSW and used for live-imaging, as described above. Hydroxyurea (HU) (Sigma) was dissolved in MFSW at 20 mM, 50 mM and 100 mM.

Definition of the start and the end of the 11th cell division
When epidermal cells begin to divide, the surface of the embryo becomes rough due to the formation of division furrows. This can be detected by the dissection microscope (OLYMPUS SZX16) and is defined as the onset of the 11th cell division. The surface of the embryo becomes smooth upon completion of epidermal cell divisions. This can also be detected by the dissection microscope and is defined as the end of the 11th cell division.

Immunohistochemistry and Phallacidin staining
For anti-dynein antibody staining, embryos were fixed in ice-cold methanol for 10 min and washed four times with 0.1% Triton X-100 in PBS (PBSTr). The fixed embryos were treated with 3% H_2O_2 in PBS for 10 min and with 50 mM NH_4Cl in PBS for 15 min. After being washed with PBS four times, the specimens were incubated for 30 min at room temperature with 0.5% blocking reagent (Roche) in PBS. Anti-dynein heavy chain antibody (R-325, Santa Cruz Biotechnology) was diluted at 1:50 in 0.5% blocking reagents in PBS, and the specimens were incubated overnight at 4°C. The primary antibody was washed with PBSTr four times. We used the MaxPO system (Nichirei Corporation) as a secondary antibody. Anti-rabbit antibody conjugated with HRP [MAX-PO (R)] was diluted at 1:20 in 0.5% blocking reagents in PBS, and the specimens were incubated overnight at 4°C. The secondary antibody was washed four times with PBSTr, and HRP activity was detected using the TSA Plus Cy3 kit (Perkin–Elmer Life Sciences) according to the manufacturer's instruction.
 To identify the lineage boundary, H2B-GFP mRNA was injected into the b4.2 cell at the 8-cell stage, and the embryos were fixed as described above. The fixed embryos were double stained with anti-dynein heavy chain antibody and anti-GFP antibody (ab13970, Abcam), as described above, with the following exception: anti-GFP antibody was diluted at 1:200 in 0.5% blocking reagents in PBS. As a secondary antibody, anti-chicken Alexa 488 antibody (A11039, Invitrogen) was diluted at 1:100 in 0.5% blocking reagents in PBS.
 To determine which side of the cell was enriched with dynein protein, specimens were squished gently to separate the cells, and cell boundaries were identified using the differential interference contrast (DIC) optics of the Zeiss LSM5 PASCAL confocal microscope.
 For Phallacidin (Thermo Fisher Scientific) staining, embryos were fixed for 30 min in 4% paraformaldehyde in a buffer containing 50 mM EGTA, 100 mM Pipes and 400 mM sucrose, adjusted to pH 6.9 (Munro and Odell, 2002a). The fixed embryos were washed three times with PBS and incubated with Phallicidin (5 unit/ml) in PBSTr either for 1 h at room temperature or overnight at 4°C and then washed three times with PBS. The embryos were treated with isopropanol series (70%, 85%, 95% and 100% in PBS) for 1 min each, and cleared with Murray clear (Benzyl Benzoate:Benzyl Alcohol = 2:1). The specimens were observed using the Zeiss LSM5 PASCAL confocal microscope.

Isolation of epidermal cell sheet
The vitelline membrane was removed manually using forceps, and the embryos were transferred to plastic dish coated with 1% agarose in MFSW. Embryos were dissected along the midline using an eyebrow hair mounted on the tip of a glass needle. Either the left side half or the right side half was used. The tissues underlying muscle and notochord cells were identified by their large cell size and cell shape. For removal of the dorsal and ventral regions, the locations of the muscle and notochord cells were employed as landmarks of the lateral region. After the removal of dorsal and ventral epidermal cells, the underlying muscle and notochord cells were removed gently with the eyebrow hair. The isolated ectodermal cell sheets were transferred gently to 2% methylcellulose in MFSW and the pattern of division was observed using the Nikon eclipse T*i*, as described above.

Image analyses and measurements

The pattern of epidermal cell division was characterized using Image J software. The A–P axis was defined as the farthest two points of the lateral side of the embryos. The long axis and short axis of cells were measured based on the best-fit ellipse using the measurement tool in Image J. The axis of division orientation (Fig. 2C) was defined as one line perpendicular to the division plane immediately on recognition of the division plane. Angles between axes, such as the A–P axis and division orientation (Fig. 2C), were measured using the angle measurement tool in Image J.

To quantify the width of the trunk and tail regions and the tail length before and after epithelial bending formation, images were obtained, in which embryos were oriented either dorsal or ventral up. Lines were drawn perpendicular to the midline at all level from anterior to posterior. Positions along the A–P axis were determined where the lines from the lateral end of the embryo to the midline were longest in the trunk and tail regions, and the lengths were defined as either width "a" for trunk or "b" for tail (Fig. 4F). Another line was drawn either coinciding with the epidermal A–P boundary visualized by a fluorescent protein injected into b4.2 in the embryo before bending formation or by connecting the deepest points of the epithelial bending on the both sides of the embryo. The length from the intersection between this line and midline to the posterior end was defined as tail length (indicated as "c" in Fig. 4F).

Two methods were used to calculate the extent of the epithelial bending. In the first method, an image was obtained in which the area of the embryo was at its maximum. Lines were drawn perpendicular to the midline at all levels from anterior to posterior (Fig. 4D, top). Positions along the A–P axis were determined where the lines from the lateral end of the embryo to the midline were either longest in the trunk region or shortest in the boundary between the trunk and tail regions, and the lengths were defined as either X or Y (Fig. 4D, top). The extent of the epithelial bending was calculated as Y/X. In the second method, a tangential line that was in contact with the trunk and tail surfaces was drawn on either lateral side of the embryo (Fig. 4D, bottom). Lines perpendicular to the tangential lines were drawn between the contact points, and the line furthest from the tangential line on the lateral side of the embryo was used to measure the extent of the epithelial bending.

To characterize the convergent extension of the notochord, embryos were stained with Phallacidin, as described above, and observed using the confocal microscope LSM5 PASCAL (Zeiss). The notochord was outlined using the polygon selection tool (Fig. 6C). A rectangle was drawn whereby each line touched the outline of the notochord. The aspect ratio of the notochord was measured as the length/width of the rectangle. A single z-section, where the aspect ratio was the maximum among other z-series, was used.

To quantify the anterior enrichment of dynein protein, the center of the cell was determined by the centroid tool in Image J (red in Fig. 5B). Three lines intersecting on the cell center were drawn: a reference axis (blue dotted lines in Fig. 5B) runs in the A-P direction; the other two with angles of 20˚ with respect to the reference axis on the both sides (fig. 5B). The signal intensity of the anterior and posterior surfaces of the cell (0.5 μm thickness) within the range between -20˚ and 20˚ was measured. The ratio of the anterior to the posterior intensities was calculated for each cell.

To quantify the fluorescent signals of DCIC-EGFP and PH-dTomato in the surface of the cells, the surface area in which the signal intensity is measured was determined as described earlier (the range between -20° and 20°). The RGB profiler tool in Image J was then used to measure the signal intensity within the determined width in all pixels from anterior to posterior approximately 2.7 μm (8 pixels) into the cell on either side of the peak of the PH-dToamato signal (Fig. 5C4). Average signal intensities of DCIC-EGFP and PH-dTomato from 26 different cell boundaries were calculated for each pixel.

Supplemental References

Miya, T., Morita, K., Suzuki, A., Ueno, N., Satoh, N., 1997. Functional analysis of an ascidian homologue of vertebrate Bmp-2/Bmp-4 suggests its role in the inhibition of neural fate specification. Development *124*, 5149–5159.

Niwano, T., Takatori, N., Kumano, G., Nishida, H., 2009. Wnt5 is required for notochord cell intercalation in the ascidian Halocynthia roretzi. Biol. Cell *101*, 645–659.

Takatori, N., Kumano, G., Saiga, H., Nishida, H., 2010. Segregation of germ layer fates by nuclear migration-dependent localization of not mRNA. Dev. Cell *19*, 589–598.